

FeSe films grown by DC sputtering from stoichiometric targets: thickness dependence of the physical properties

M. V. Ale Crivillero¹, M. L. Amigó^{1*}, N. Haberkorn¹, G. Nieva¹, L. Avilés², M. Sirena², S. Suárez³ and J. Guimpel¹

¹División Bajas Temperaturas, Centro Atómico Bariloche, CNEA - CONICET - Instituto Balseiro, UNCuyo y CNEA, (8400) Bariloche, Argentina.

²División Resonancias Magnéticas, Centro Atómico Bariloche, CNEA - CONICET - Instituto Balseiro, UNCuyo y CNEA, (8400) Bariloche, Argentina.

³División Colisiones Atómicas y Física de Superficies, Centro Atómico Bariloche, CNEA - CONICET - Instituto Balseiro, UNCuyo y CNEA, (8400) Bariloche, Argentina.

*Current address: Institute for Solid State Research, IFW Dresden, Germany.

E-mail: victoria.ale@ib.edu.ar

January 2018

Abstract. In this work, we study thickness effects in the structural and electronic properties of β -FeSe films grown by sputtering. We report a superconductor-insulator transition (SIT) as a function of thickness, for films in different substrates (SrTiO₃, MgO and Si) in a wide range of growth temperatures. As the thickness increases the evolution of the structural properties and morphology is not trivial, which can be associated to a strained initial growth. In the limit of textured thick films, the critical temperature takes values slightly higher than the expected for bulk β -FeSe, $T_c \simeq 12$ K, probably owing to growth associated stress. The electronic structure was explored by performing magnetotransport and Hall effect experiments, finding features associated to the tetragonal-to-orthorhombic structural phase transition.

PACS numbers: 81.15.Cd, 74.25.F-, 74.70.Xa

Keywords: Thin Films, FeSe, Sputtering

1. Introduction

Among the iron based superconductors, iron selenide has the simplest crystal structure. This makes this material a good candidate for basic studies, like exploring the mechanisms of high temperature superconductivity and competition between magnetic and superconducting phases. Despite the structural simplicity, high quality single crystals were obtained only years after its discovery [1][2]. Interesting behavior has been reported in this material such as a strong enhancement of the critical temperature with pressure (hydrostatic [3][4] or residual stress [5][6]), multi-band electronic structure [7][8], orthorhombic [9] and nematic phase transitions at 90 K [10][11]. Several theoretical scenarios have been proposed like frustrated magnetism [12], nematicity driven by orbital [13] or spin [14] degrees of freedom, CDW [15] and SDW [16].

Particular interest has motivated the growth of thin films of FeSe for potential technical applications [17]. Thin films of FeSe have been synthesized by different growth methods such as pulsed laser deposition (PLD) [5][6][18][19], molecular beam epitaxy (MBE) [3][16][20][21] and in a lesser extent by sputtering [22][23][24][25]. The discovery of high-temperature superconductivity over 65 K in extremely thin FeSe films [21][26] have triggered considerable experimental and theoretical efforts in order to elucidate the underlying mechanism [16][27][28][29]. In this context, fundamental questions concerning the interfacial effects as a function of thickness are still open.

In this work, we report on the fabrication of thin films of β -FeSe by DC magnetron sputtering from stoichiometric targets, with the aim to study the influence of the growth condition on the superconducting properties. We systematically studied growth parameters such as substrate temperature, Ar pressure and substrate to target distance. We have focused the present report on the influence of substrate temperature, T_s , and film thickness, t , on physical properties. The phase purity and crystal structure of the films were characterized by X-ray diffraction measurement (XRD). The surface morphology was studied using a Scanning Electron Microscope (SEM) and an Atomic Force Microscope (AFM). The local chemical composition was measured by Energy-Dispersive X-ray Spectroscopy (EDX) and Rutherford Backscattering Spectrometry (RBS). We carried out electrical transport measurements with magnetic fields up to 16 T.

2. Experimental details

Fe_{1-x}Se thin films have been deposited by DC magnetron sputtering starting from a stoichiometric FeSe target. The target was fabricated from Fe (99.95 %) and Se (99.999 %) grits. Two consecutive

cycles of mixing, heating up to 430 °C for 48 hours and milling were performed to achieve solid state reaction of the powder. In a final process the powder was pressed and sintered at 430 °C for 4 days. X-ray diffraction of the powder was performed at each stage to characterize the material. The final target material was β -FeSe with approximately 1.5 % γ - Fe_7Se_8 . A very small amount, <5 %, of FeO was also observed.

Films were grown onto SrTiO_3 (100), MgO (100) and Si (100) substrates, labelled from now on as STO, MgO and Si. They were attached to a resistive heater [30] with Ag paste, which allowed for heating up to a nominal temperature of 680 °C. The substrate temperature, T_s , was measured and controlled with a thermocouple in direct thermal contact with the substrates. Base pressure of the sputtering system was 3×10^{-6} Torr. The growth parameters that were kept constant for all films are sputtering gas, 99.999% pure Ar, and pressure, 45 mTorr, target power, 8 W for a 1.5" diameter target, and target to substrate distance, at 5 cm. These parameters were found to be optimal in previous, unreported tests. The influence of T_s and film thickness, t , was studied by growing films at T_s between 200 °C and 680 °C and for total growth time between 5 and 30 min.

The chemical composition of the films has been routinely measured by EDX and for some samples also by Rutherford Backscattering Spectrometry (RBS). Under the conditions described above, all the samples have composition close to the expected values, i.e. Fe:Se \approx 1. The homogeneity of the films was also investigated. No spatial variations were found within the error in EDX analysis.

The thickness of the films was measured by contact profilometry in a well defined sample step. This step was generated by first masking part of the substrate with silver epoxy, growing the film, and finally removing the epoxy. For thin films, the thickness was also determined through low angle X-Ray reflectivity, XRR, measuring the periodicity of the Kiessig fringes [31], observed as intensity oscillations, figure 1. When the later were observed, both methods of thickness determination coincided within 10 %.

The XRD and XRR patterns were measured at room temperature on a PANalytical Empyrean diffractometer in Bragg-Brentano geometry with Cu K_α radiation, wavelength $\lambda = 1.5418$ Å. The samples were mounted in a 4-circle Eulerian cradle, which allowed for precise alignment. Due to physical limitations of the Eulerian cradle, a monochromator could not be used. Instead, a Ni filter was used to diminish the Cu K_β radiation. For the extremely intense substrate diffraction, the K_β peak and the Ni absorption edge are visible in the data, the later as a step-like discontinuity in the background intensity

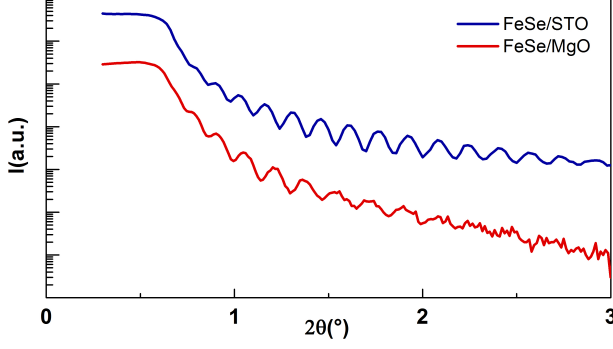


Figure 1. Low angle X-ray reflectometry (XRR) for β -FeSe thin films ($t \sim 60$ nm) deposited on SrTiO_3 (blue line) and MgO (red line).

between the K_α and K_β peaks.

Electrical transport properties were measured in a standard 4 probe geometry, defined by UV photolithography and ion milling. For the Hall effect measurements, two probes at both sides of the current carrying line were added. The measurements were performed in an Oxford cryostat equipped with an 18 T superconducting coil and sample rotation capability, in the 1.8 K to 300 K range.

3. Results and discussion

3.1. Crystalline structure and surface morphology

Figure 2 shows the diffraction spectra for films grown onto STO, MgO and Si. The growth parameters used for each substrate correspond to those who maximize the superconducting properties, see section 3.2. For the film grown onto STO the more intense peaks can be indexed as the (001) β -FeSe family. The rocking curve of the (001) peak has a full width at half maximum (FWHM) of approximately 5° , indicating textured growth. Also, smaller peaks corresponding to (101) β -FeSe and (001) γ -Fe₇Se₈ are observable. These results indicate preferred c-axis growth, coexisting with a small quantity of (101) β -FeSe and (001) γ -Fe₇Se₈ domains. In the case of the film grown onto MgO, figure 2b, only peaks that can be indexed as (101) _{β} and (004) _{γ} are observed. The presence of the β -FeSe phase is confirmed by the diffraction pattern taken at azimuthal angle $\chi = 55.8^\circ$, showed in the inset, where the (001) _{β} peak is observed. In this case, the rocking curve shows a narrower peak. On the other hand, on Si substrates, single-phase films with preferred c-axis growth can be obtained (figure 2c).

Figure 3a shows the azimuthal ϕ scans for the (101) β -FeSe diffraction peak of films grown on STO. The vertical dashed lines show the position of the measured peaks in an azimuthal scan for the (101)

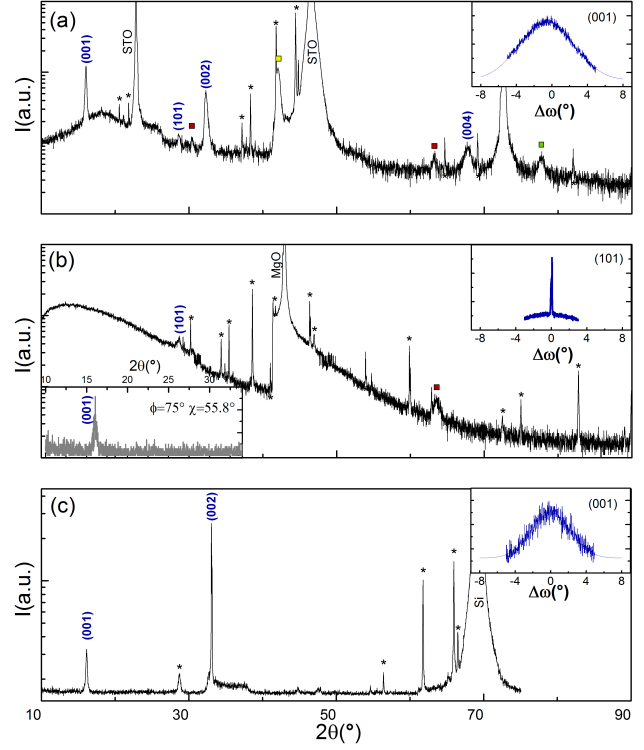


Figure 2. XRD pattern of β -FeSe films grown onto STO(a), MgO(b) and Si(c). The (001) peaks associated to the β -FeSe phase are clearly observed. The red labels correspond to (001) γ -Fe₇Se₈. The yellow label could be either indexed as (102) γ -Fe₇Se₈ or (200) FeO, while the green label might be identify as (203) γ -Fe₇Se₈. The asterisk signs stand for substrate related peaks. The right insets show the corresponding rocking curve: (a) and (c) (001) _{β} reflexion and (b) (101) _{β} reflexion. For MgO, also the $\theta - 2\theta$ diffraction pattern taken at azimuthal angle $\chi = 55.8^\circ$ is showed in the left inset, where the peak β -FeSe (001) is observed. The growth parameters are: (a) $T_s = 530^\circ\text{C}$ and $t = 400$ nm, (b) $T_s = 480^\circ\text{C}$ and $t = 185$ nm and (c) $T_s = 550^\circ\text{C}$ and $t = 350$ nm.

diffraction of the STO substrate. The figure includes data for films grown at $T_s = 530^\circ\text{C}$ with thicknesses $t = 60$ nm and $t = 400$ nm, a film grown at $T_s = 360^\circ\text{C}$ with $t = 55$ nm and a film grown at $T_s = 480^\circ\text{C}$ with $t = 380$ nm. It is clear that the thinner films present an in-plane alignment with the [100] β -FeSe axis parallel to the [100] STO, being optimized for $T_s = 360^\circ\text{C}$. However, as the film grows thicker, this orientation rotates being the [110] β -FeSe parallel to the [100] STO. This may be indicative of an initially very stressed cube-on-cube growth, which relaxes after a critical thickness by rotating 45° around the vertical axis.

In the case of thick films grown on MgO, figure 3b, the azimuthal scan of the (001) reflection shows a 30° periodicity and was found at $\pm 45^\circ$ to the (202) reflexions of the substrate, i.e. parallel to the MgO [110]. The rest of the peaks may indicate the existence of twin boundaries generated by 30°

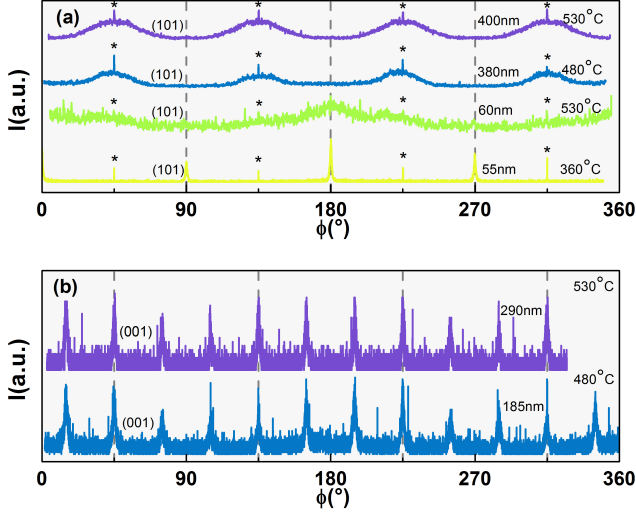


Figure 3. a) Azimuthal ϕ scans for the (101) β -FeSe diffraction peak of films grown on STO. The vertical dashed lines show the position for the [100] axis of the STO and the asterisks correspond to spurious peaks associated to the substrate. The data correspond to thin films ($t \sim 55$ and 60 nm) growth at $T_s = 360^\circ\text{C}$ and $T_s = 530^\circ\text{C}$. For the thick films ($t \sim 380$ and 400 nm) the substrate temperature was $T_s = 480^\circ\text{C}$ and $T_s = 530^\circ\text{C}$. b) Azimuthal ϕ scans for the (001) β -FeSe diffraction peak of films grown on MgO. The vertical dashed lines show the [110] directions for MgO. The figure includes data for thick films, $t \sim 185$ nm and $t \sim 290$ nm, grown at $T_s = 480^\circ\text{C}$ and $T_s = 530^\circ\text{C}$, respectively.

rotation of the β -FeSe unit cell around the MgO [001] direction. The 30° rotation matches with the angle $\alpha = \arctan(a/\sqrt{a^2 + c^2}) \sim 30^\circ$ between the rectangle side and diagonal. The films were grown at $T_s = 480^\circ\text{C}$ and $T_s = 530^\circ\text{C}$ with thicknesses of $t = 185$ nm and $t = 290$ nm.

The surface roughness and morphology have been characterized by AFM and SEM, respectively. The topography of most of the films that present superconductivity shows a tweed grain pattern with a characteristic length around $1\mu\text{m}$, see for example figures 4c, 4d and 4g. In contrast, thin films grown at low temperature ($T_s = 360^\circ\text{C}$, figures 4a and 4e) present a smoother surface but, as we will see in the next section, are not superconducting. The complex evolution of the morphology can also be emphasized taking into account the dependence of the roughness on the thickness for different types of substrates. The plot in figure 4h shows surface roughness as a function of nominal thickness for films grown on STO and MgO at 530°C . For the thinnest samples, roughness is comparable to thickness. It decreases with increasing t for films grown on MgO. For films grown on STO, roughness seems to be independent of t .

Our results show that as the thickness decreases the evolution of the structural properties and morphology of β -FeSe films grown by sputtering is non-trivial.

The out of plane alignment and roughness are strongly dependent on thickness, T_s and type of substrate. This implies that a comprehensive study of these properties is essential to understand the thickness influence on transport properties.

3.2. Electrical transport properties

3.2.1. Superconductor-insulator transition (SIT)

Figure 5 shows the normalized electrical resistivity, $\rho(T)/\rho(250\text{ K})$, as a function of temperature, T , for films of different thicknesses. Films were grown at $T_s = 530^\circ\text{C}$ under equivalent conditions onto substrates of STO or MgO. The thicknesses vary from 60 to 400 nm for STO and from 50 to 290 nm for MgO for deposition times between 5 and 30 min. A change from insulating to superconducting behavior is observed as the film thickness increases, indicating a superconductor-insulator transition (SIT) [22] [32]. For growth temperature $T_s = 530^\circ\text{C}$, the critical thickness is between 100 and 200 nm.

To study the influence of the growing temperature in the superconductor-insulator transition, we present $\rho(T)/\rho(250\text{ K})$ for films grown at different T_s on STO, MgO and Si in figure 6. For clarity, the results have been separated for thin, $50 \leq t \leq 60$ nm, and thick, $300 \leq t \leq 400$ nm films. For the thinner films, regardless of the substrate, an insulating-like behavior is observed for almost all T_s studied. In the case of thicker films grown on STO or MgO, a metallic like behavior is observed followed by a superconductor transition at low temperatures, the only exception being presented by the films grown with $T_s \leq 300^\circ\text{C}$. In Si substrates, for $T_s \sim 500^\circ\text{C}$ only a transition onset is found at low temperatures. Both for higher and lower T_s , insulating character is found. These results show that the SIT on decreasing thickness is observed in a wide range of T_s independently of the substrate, proving to be a general feature of β -FeSe films grown by sputtering.

We emphasize the superconducting properties dependence on the growth parameters. For STO substrates the optimal results, i.e. highest superconducting transition, T_c , and sharper transition, are found for $T_s = 530^\circ\text{C}$, with $T_c \simeq 12\text{ K}$ and transition width $\Delta T_c \simeq 4\text{ K}$. For MgO substrates $T_c \simeq 12\text{ K}$ is found, in a range of $360^\circ \leq T_s \leq 480^\circ\text{C}$ but with a broader transition, incomplete down to 1.8 K . These values of T_c are slightly higher than the previously reported for films obtained by sputtering [22], [23], [25] and are similar to those that have been reported for crystals with nanoscale intergrowth of β -FeSe and γ -Fe₇Se₈ [33].

There are previous report on SIT for FeSe films [22] [32]. This kind of behavior for the case of MgO substrates have been discussed within a disordered granular superconductor scenario [22] where

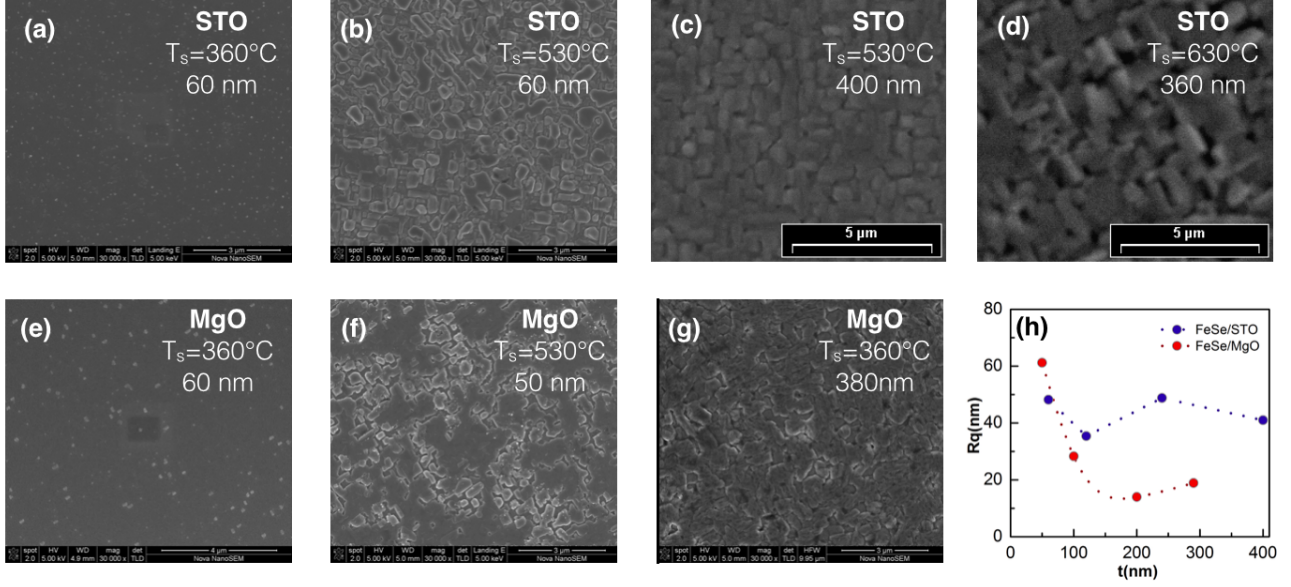


Figure 4. (a)-(g): SEM images of representative samples grown under different conditions. (h): The plot shows the root mean square (RMS) surface roughness, R_q , as a function of nominal thickness for films grown onto STO and MgO at $T_s = 530^\circ\text{C}$.

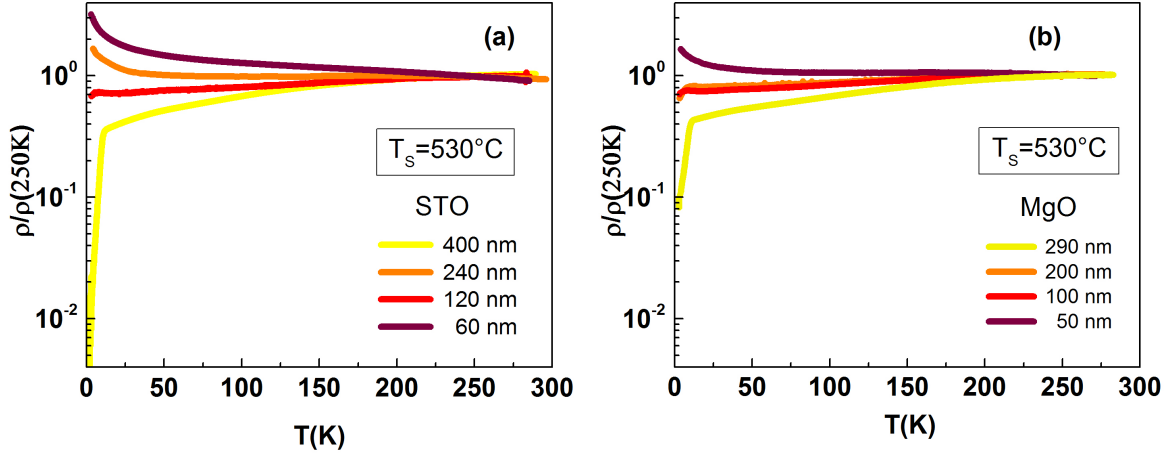


Figure 5. Normalized resistivity ($\rho(T)/\rho(250\text{K})$) as function of temperature for films grown onto (a) STO and (b) MgO substrates with thickness as a parameter.

the disorder associated to smaller thickness induces a superconductor-insulator transition. Nevertheless, the proposed scheme become inappropriate for our samples on the basis of the results presented in the previous section. Our structural data suggest a strained initial growth characterized by an epitaxial nature, enhanced in the case of STO substrate and $T_s = 360^\circ\text{C}$, which evolve to a granular morphology in the case of thicker films, in contrast to the strong c-axis texture irrespective of the film thickness reported by Schneider et al [22].

An integral proposal to understand this phenomenology must be able to explain which is the origin of the insulating behavior despite having the tetragonal

phase with a low deposition time and the enhancement of the critical temperature with respect to the bulk in the thicker samples. A plausible scenario is a Stranski-Krastanov layer-plus-island growth mode where preferentially oriented grains coalesce at a critical thickness with an underlying non-superconducting sheet. In this scenario, the stress associated to the grains coalescence and/or nanoscale intergrowth of $\beta\text{-FeSe}$ and $\gamma\text{-Fe}_7\text{Se}_8$ may play a key role in the transport properties.

3.2.2. Normal state Figure 7 shows $\rho(T)$ for optimal superconducting samples on STO substrate ($T_s = 530^\circ\text{C}$, $t \sim 400$ nm) and MgO substrate ($T_s = 360^\circ\text{C}$, $t \sim 380$ nm). Besides the obvious superconducting

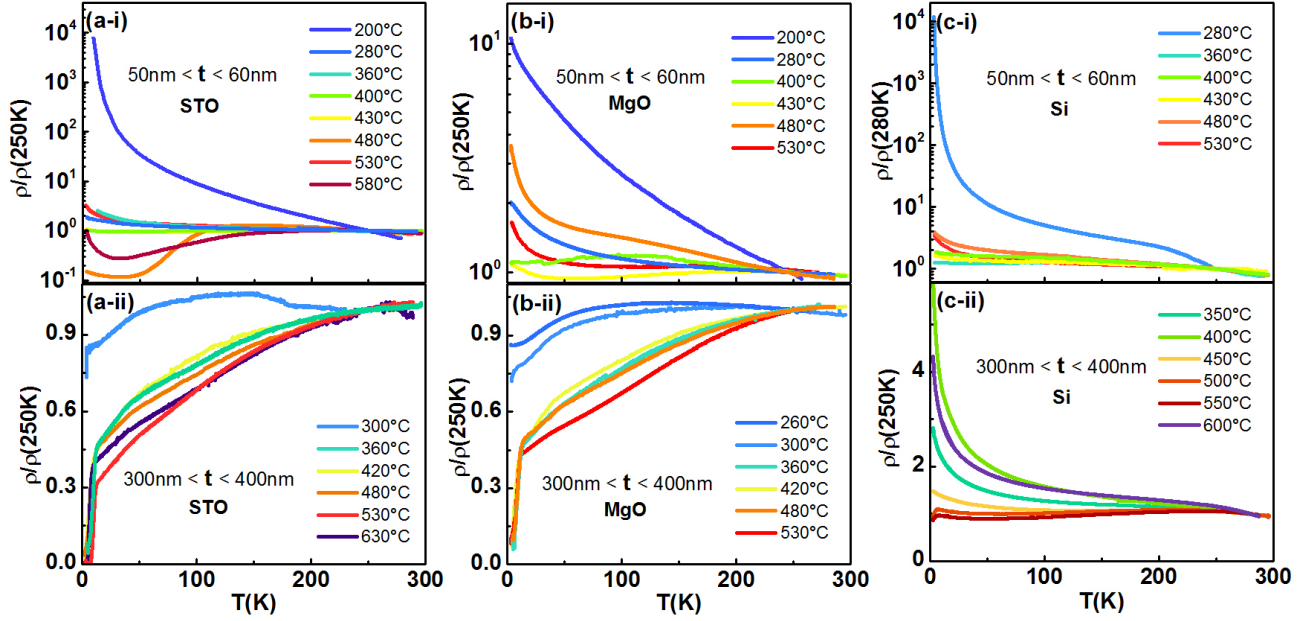


Figure 6. Normalized resistivity, $\rho(T)/\rho(250K)$, for films grown at different T_s on STO (a), MgO (b) and Si (c). For clarity, the results have been separated according to the thickness range: (i) thin films ($50 \leq t \leq 60$ nm) and (ii) thick films ($300 \leq t \leq 400$ nm).

transition, in both cases the data shows a slope change indicating the structural transition for β -FeSe around 100 K [9]. This feature is zoomed in the lower inset of figure 7a, together with $d\rho/dT$. In this inset is also included the data for magnetic field of 16 T applied perpendicular to the substrate surface. As observed also in bulk single crystals [34], a positive magnetoresistance is observed below the structural transition, slightly higher in the case of MgO substrate.

More information on the electronic structure is obtained from Hall-effect measurements. The upper inset in figure 7a shows the T dependence of the Hall coefficient, which has been measured with two different protocols. The first one corresponds to the usual 4-probe transversal voltage ρ_{xy} vs H experiment. The Hall coefficient R_H is determined from the $\rho_{xy}(H)$ data, being $R_H = \rho_{xy}/H$ in the case of a linear dependence. The second one, labelled as *method 2*, relies on the fact that for a thin film, only the perpendicular component of H originates a transversal voltage. Consequently, in an angular dependence experiment at constant H , R_H is obtained from the slope of ρ_{xy} vs $H \sin(\theta)$. Also, the result obtained from the antisymmetric signal of $\rho_{xy}(T)/H$ is presented, where $\rho_{xy}(T) = [\rho_{xy}(T, H) - \rho_{xy}(T, -H)]/2$.

In both cases, upper insets in figures 7a and 7b, R_H takes positive values close to zero above the structural transition showing a sign reversal to negative values for $T < T^*$, with $T^* \sim 90$ K. This change of sign is reminiscent of the ones presented by single crystals close to the transition, which has been associated with the structural distortion and originating in the

multiband character of β -FeSe [8] [35]. Nevertheless, there are striking differences at low temperatures such as: (i) our films present a linear Hall effect up to 16 T, in contrast to the nonlinear behavior observed below T^* in high quality single crystals [8], (ii) the minimum at $T \sim 20$ K [35], interpreted as due to a pseudogap formation in Ref. [36], is not observed. We emphasize that despite the presence of disorder in our samples some features associated with nematic fluctuations like a change in the sign of Hall coefficient and a concomitant positive magnetoresistance are clearly observed in magnetotransport and Hall experiments. Overall, the differences found may shed light on what aspects of bulk single crystals are more susceptible to disorder.

3.2.3. Superconducting properties Regarding the superconducting properties, insets in figure 8 show the evolution of the transition for the previous films with applied magnetic field parallel and perpendicular to the substrate surface. From these curves the perpendicular and parallel critical fields, $\mu_0 H_{c2\perp}(T)$ and $\mu_0 H_{c2\parallel}(T)$ are defined, which are shown in the respective main figures. Since a coherence length ~ 5 nm, which can be obtained from these fields, is much less than the film thickness and roughness, we interpreted the difference between $\mu_0 H_{c2\perp}(T)$ and $\mu_0 H_{c2\parallel}(T)$ as due to the intrinsic β -FeSe anisotropy. From the slope of $\mu_0 H_{c2}(T)$ in the vicinity of T_c and using the WHH model [37], the values of $\mu_0 H_{c2}(T = 0)$ are estimated.

In the case of STO, figure 8a, the parallel and perpendicular configurations corresponds principally

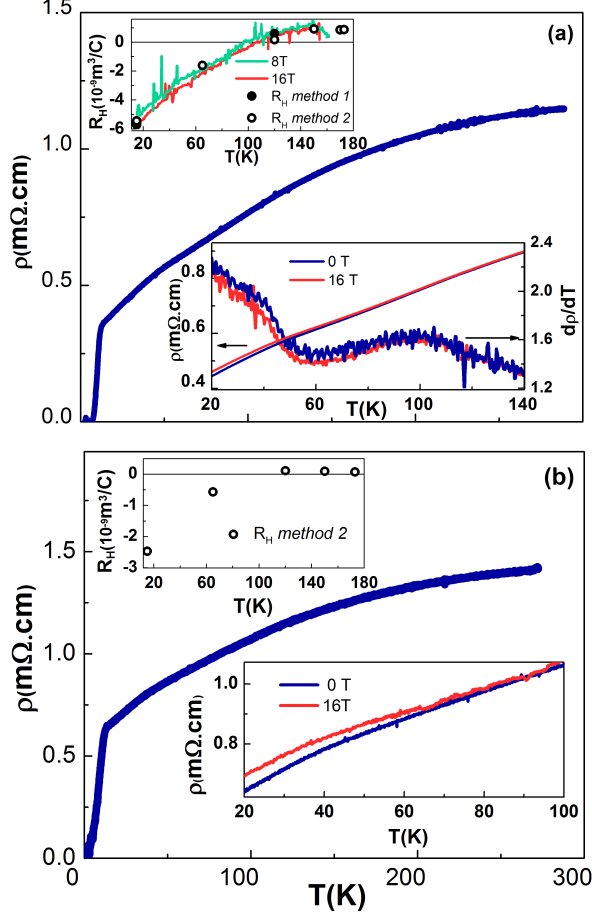


Figure 7. In plane resistivity against temperature of superconducting films grown onto (a) STO and (b) MgO. For each plot, the lower inset presents a zoom around the structural transition including data with applied magnetic field. The upper inserts show the measured Hall coefficient along with ρ_{xy}/H as a function of T .

to magnetic field along the ab plane and c axis, respectively. The values of $\mu_0 H_{c2}(T=0)$ are estimated as $\mu_0 H_{c2\perp}(0) = (18.0 \pm 0.5) \text{ T}$ and $\mu_0 H_{c2\parallel}(0) = (34.4 \pm 0.5) \text{ T}$, in accordance with the previously reported values [5][38]. The anisotropy defined as $\gamma = H_{c2\parallel}(T)/H_{c2\perp}(T)$ takes a maximum value of 2.4 at 11.6 K and decreases for lower temperatures. These values are probably underestimated due to the presence of misaligned grains, but they are not far from the reported values. From the Ginzburg Landau relations for 3D superconductor in the clean limit [17], the estimated values for coherence lengths at zero temperature are $\xi_{ab}(0) \sim 4.3 \text{ nm}$ and $\xi_c(0) \sim 2.2 \text{ nm}$.

4. Conclusions

In summary, we report on the superconductor-insulator transition (SIT) induced by reducing the thickness of β -FeSe films grown by sputtering, which seems

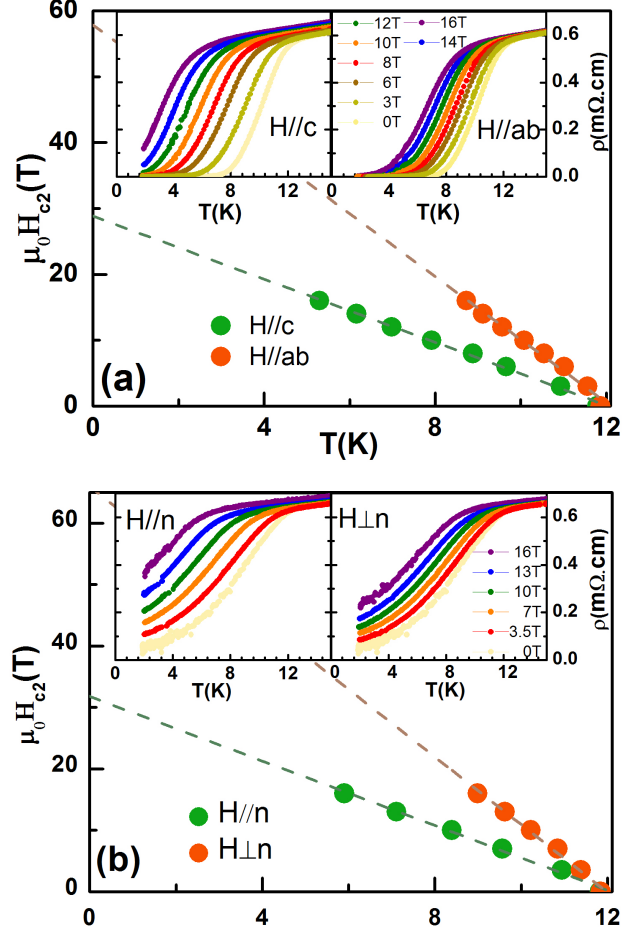


Figure 8. Superconducting phase diagrams, $\mu_0 H_{c2\perp}$ and $\mu_0 H_{c2\parallel}$, for films grown onto (a) STO and (b) MgO. A magnetic field up to 16 T was applied parallel and perpendicular to the substrate surface. Insets show the superconducting transitions as a function of H .

to be a general feature of β -FeSe films grown by sputtering. We have focused the present investigation on the evolution of the morphology and structural properties as the thickness decreases finding evidence of an initially very stressed growth, which relaxes by rotation of the structure with respect to the substrate axis after a critical thickness.

These results imply that the scheme of induction of disorder for thinner films is inappropriate. A plausible scenario is a layer-plus-island growth where preferentially oriented grains coalesce at a critical thickness with an underlying non-superconducting sheet.

In the limit of textured thick films, our samples allow us to discern whether the presence of disorder is relevant for some physical properties. The critical temperature ($T_c \sim 12 \text{ K}$) takes values slightly higher than the expected for bulk β -FeSe, $T_c = 9 \text{ K}$. This enhancement could be related to a nanoscale

intergrowth of β -FeSe and γ -Fe₇Se₈ and/or stress associated to grain coalescence. On the other hand, superconducting properties like anisotropy and coherence length takes values in good accordance with those reported for high quality epitaxial thin films. Regarding the electronic structure in the normal state, despite the presence of impurity phases and disorder, features associated to nematic fluctuations are clearly observed in magnetotransport and Hall experiments.

5. Acknowledgements

We thank P. Troyón and M. Corte at CM-GIA-GAATEN-CNEA for SEM/EDX characterization. Work partially supported by Conicet PIP 2014-0164, ANPCyT PICT 2014-1265 and Sectyp UNCuyo 06/C441 and 06/C504.

References

- [1] F.-C. Hsu, J.-Y. Luo, K.-W. Yeh, T.-K. Chen, T.-W. Huang, P. M. Wu, Y.-C. Lee, Y.-L. Huang, Y.-Y. Chu, D.-C. Yan, and M.-K. Wu, *PNAS* 105, 105, 14 262 (2008).
- [2] D. Chareev, E. Osadchii, T. Kuzmicheva, J.-Y. Lin, S. Kuzmichev, O. Volkov and A. Vasiliev, *CrystEngComm* 1,15, 1989 (2013).
- [3] J.P. Sun, K. Matsuura, G.Z. Ye, Y. Mizukami, M. Shimozawa, K. Matsubayashi, M. Yamashita, T. Watashige, S. Kasahara, Y. Matsuda, J.-Q. Yan, B.C. Sales, Y. Uwatoko, J.-G. Cheng and T. Shibauchi, *Nat. Commun.* 7, 12146 (2016).
- [4] S. Medvedev, T. M. McQueen, I. A. Troyan, T. Palasyuk, M. I. Erements, R. J. Cava, S. Naghavi, F. Casper, V. Ksenofontov, G. Wortmann, and C. Felser, *Nature Materials* 8, 630 (2009).
- [5] F. Nabeshima, Y. Imai, M. Hanawa, I. Tsukada and A. Maeda, *Appl. Phys. Lett.* 103, 172602 (2013).
- [6] Y. Imai, Y. Sawada, D. Asami, F. Nabeshima and A. Maeda, *Physica C* 530, 24, (2016).
- [7] H. Lei, D. Graf, R. Hu, H. Ryu, E. S. Choi, S.W. Tozer and C. Petrovic, *Phys. Rev. B* 85, 094515 (2012).
- [8] M. D. Watson, T. Yamashita, S. Kasahara, W. Knafo, M. Nardone, J. Bard, F. Hardy, A. McCollam A. Narayanan, S. F. Blake, T. Wolf, A. A. Haghighirad, C. Meingast, A. J. Schofield, H. v. Lhneysen, Y. Matsuda, A. I. Coldea and T. Shibauchi, *Phys. Rev. Lett.* 115, 027006 (2015).
- [9] McQueen T M, Williams A J, Stephens P W, Tao J, Zhu Y, Ksenofontov V, Casper F, Felser C and Cava R J, *Phys. Rev. Lett.* 103(5) 057002 (2009).
- [10] A. E. Böhmer, F. Hardy, F. Eilers, D. Ernst, P. Adelmann, P. Schweiss, T. Wolf and C. Meingast, *Phys. Rev. B* 87, 180505(R) (2013).
- [11] A. E. Böhmer, T. Arai, F. Hardy, T. Hattori, T. Iye, T. Wolf, H. v. Lhneysen, K. Ishida, and C. Meingast, *Phys. Rev. Lett.* 114, 027001 (2015).
- [12] R. Yu and Q. Si, *Phys. Rev. Lett.* 115, 116401 (2015).
- [13] S.-H. Baek, D. V. Efremov, J. M. Ok, J. S. Kim, J. van den Brink and B. Bchner, *Nature materials* 14, 210 (2015).
- [14] Q. Wang, Y. Shen, B. Pan, Y. Hao, M. Ma, F. Zhou, P. Steffens, K. Schmalzl, T. R. Forrest, M. Abdel-Hafiez, X. Chen, D. A. Chareev, A. N. Vasiliev, P. Bourges, Y. Sidis, H. Cao and J. Zhao, *Nature Materials* 15, 159 (2016).
- [15] A. Chubukov, R. Fernandes and J. Schmalian, *Phys. Rev.* 91, 201105(R) (2015).
- [16] S. Tan, Y. Zhang, M. Xia, Z. Ye, F. Chen, X. Xie, R. Peng, D. Xu, Q. Fan, H. Xu, J. Jiang, T. Zhang, X. Lai, T. Xiang, J. Hu, B. Xie and D. Feng, *Nature Materials* 12, 634 (2013).
- [17] S. Haindl, M. Kitzun, S. Oswald, C. Hess, B. Buchner, L. Skolling, L. Wilde, T. Thersleff, V. V. Yurchenko, M. Jourdan, H. Hiramatsu and H. Hosono, *Rep. Prog. Phys.* 77, 046502 (2014).
- [18] Y. F. Nie, E. Brahimi, J. I. Budnick, W. A. Hines, M. Jain, and B. O. Wells, *Appl. Phys. Lett.* 94, 242505 (2009).
- [19] Ta-Kun Chen, Jiu-Yong Luo, Chung-Ting Ke, Hsian-Hong Chang, Tzu-Wen Huang, Kuo-Wei Yeh, Chung-Chieh Chang, Po-Chun Hsu, Chun-Te Wu, Ming-Jye Wang and Mau-Kuen Wua, *Thin Solid Films* 519, 1540 (2010).
- [20] C.-L. Song, Y.-L. Wang, P. Cheng, Y.-P. Jiang, W. Li, T. Zhang, Z. Li, K. He, L. Wang, J.-F. Jia, H.-H. Hung, C. Wu, X. Ma, X. Chen, Q.-K. Xue, *Science* 332, 1410 (2011).
- [21] D. Liu, W. Zhang, D. Mou, J. He, Y.-B. Ou, Q.-Y. Wang, Z. Li, L. Wang, L. Zhao, S. He, Y. Peng, X. Liu, C. Chen, Li Yu, G. Liu, X. Dong, J. Zhang, C. Chen, Z. Xu, J. Hu, X. Chen, X. Ma, Q.-K. Xue and X.J. Zhou, *Nat. Commun.* 3, 931 (2012).
- [22] R. Schneider, A. G. Zaitsev, D. Fuchs, and H. v. Lohneysen, *Phys. Rev. Lett.* 108, 257003 (2012).
- [23] R. Schneider, A. G. Zaitsev, D. Fuchs and R. Fromknecht, *Supercond. Sci. Technol.* 26, 055014 (2013).
- [24] S. Speller, C. Aksoy, M. Saydam, H. Taylor, G. Burnell, A. Boothroyd and C. Grovenor, *Supercond. Sci. Technol.* 24, 075023 (2011).
- [25] E. Venzmer, A. Kronenberg and M. Jourdan, *J Supercond Nov Magn* 29, Issue 4, 897-903 (2016).
- [26] Q.Y. Wang, Z. Li, W.H. Zhang, Z.C. Zhang, J.S. Zhang, W. Li, H. Ding, Y.B. Ou, P. Deng, K. Chang, J. Wen, C.L. Song, K. He, J.F. Jia, S.H. Ji, Y.Y. Wang, L.L. Wang, X. Chen, X.C. Ma and Q.K. Xue, *Chin. Phys. Lett.* 29, 37402 (2012).
- [27] J. J. Lee, F. T. Schmitt, R. G. Moore, S. Johnston, Y.-T. Cui, W. Li, M. Yi, Z. K. Liu, M. Hashimoto, Y. Zhang, D. H. Lu, T. P. Devereaux, D.-H. Lee and Z.-X. Shen, *Nature* 515, 245 (2014).
- [28] Y.-Y. Xiang, F. Wang, D. Wang, Q.-H. Wang, and D.-H. Lee, *Phys. Rev. B* 86, 134508 (2012).
- [29] T. Bazhiron and M. L. Cohen, *J. Phys.: Condens. Matter* 25, 105506 (2013).
- [30] F. Pardo, G. Burmeister and J. Guimpel, *Rev. Sci. Instrum.* 67, 2370 (1996).
- [31] H. Kiessig, H. Kiessig, Interferenz von Röntgenstrahlen an dünnen Schichten, *Annalen der Physik* 402 (7), 769?788 (1931) doi:10.1002/andp.19314020702.
- [32] Q. Wang, W. Zhang, Z. Zhang, Y. Sun, Y. Xing, Y. Wang, L. Wang, X. Ma, Q.-K. Xue and J. Wang, *2DMater.* 2, 044012 (2015).
- [33] M. L. Amigó, M. V. Ale Crivillero, D. G. Franco, A. Badía-Majós, J. Guimpel, J. Campo, F. Damay, F. Porcher, A. M. Condó and G. Nieva, *Supercond. Sci. Technol.* 30, (2017).
- [34] M. L. Amigó, V. Ale Crivillero, D. G. Franco and G. Nieva, *J. Phys.: Conf. Ser.* 568, 022005 (2014).
- [35] S. Kasahara, T. Watashige, T. Hanaguri, Y. Kohsaka, T. Yamashita, Y. Shimoyama, et al, *PNAS* 111(46), 16309, (2014).
- [36] S. Kasahara, T. Yamashita, A. Shi, R. Kobayashi, Y. Shimoyama, T. Watashige, K. Ishida, T. Terashima, T. Wolf, F. Hardy, C. Meingast, H. v. Lohneysen, A. Levchenko, T. Shibauchi and Y. Matsuda, *Nat. Commun.* 7:12843 (2016).
- [37] N. R. Werthamer, E. Helfand, and P. C. Hohenberg, *Phys.*

- Rev.*147, 295 (1966).
- [38] T. Terashima, K.Kikugawa, A. Kiswandhi, E Choi, J. Brooks, S. Kasahara, T. Watashige, H. Ikeda,T. Shibauchi, Y. Matsuda,T. Wolf, A. Bhmer, F. Hardy, C. Meingast, H. Löhneysen, M. Suzuki, R. Arita and S. Uji, *Phys. Rev. B* 90, 144517 (2014).